Heliyon 9 (2023) e21755

Contents lists available at ScienceDirect

Heliyon

journal homepage: www.cell.com/heliyon

D-tyrosine enhances disoctyl dimethyl ammonium chloride on alleviating SRB corrosion

Jingyi Zhou [a], Hongyi Li [a], Shichu Gong [a], Shuguang Wang [a,b,c,d], Xianzheng Yuan [a,b], Chao Song [a,b,*]

[a] Shandong Key Laboratory of Water Pollution Control and Resource Reuse, School of Environmental Science and Engineering, Shandong University, Qingdao, Shandong, 266237, China
[b] Shandong Key Laboratory of Environmental Processes and Health, School of Environmental Science and Engineering, Shandong University, Qingdao, Shandong, 266237, China
[c] Sino-French Research Institute for Ecology and Environment (ISFREE), School of Environmental Science and Engineering, Shandong University, Qingdao, Shandong, 266237, China
[d] WeiHai Research Institute of Industrial Technology of Shandong University, Weihai, 264209, China

ARTICLE INFO

Keywords:
Microbiologically influenced corrosion
Sulfate reducing bacteria
Corrosion inhibition
Biofilm
D-amino acid

ABSTRACT

Microbiologically influenced corrosion (MIC) caused by sulfate reducing bacteria (SRB) is a serious challenge in many industries, but biofilm greatly decreases the toxicity of bactericides to cell inside. D-amino acids are potential enhancers for bactericides due to their excellent performance on biofilm inhibition. However, the mechanism of D-amino acid cooperating with bactericides for MIC inhibition is still unknown. In this study, D-tyrosine (D-Tyr) and disoctyl dimethyl ammonium chloride (DDAC) were selected as the typical D-amino acid and bactericide, respectively, to evaluate their synergetic inhibition on the corrosion caused by *Desulfovibrio vulgaris*. D-Tyr obviously enhanced the role of DDAC in inhibiting corrosion with high corrosion inhibition efficiency at 77.23 %. The attachment of EPS and live cells on the coupon surface decreased in the presence of D-Try, leading to more cells directly exposed to DDAC. Besides, D-Try decreased the amount of live cells on the surface and thus reduced the utilization of Fe by SRB and corrosion current. Moreover, dead cells settling to the coupon surface may form a protective lay to retard the contact between live SRB and Fe, leading to slow cathode reaction and less corrosion. Therefore, D-Tyr can reduce the coverage of biofilm, thereby reducing its protective effect on SRB and achieving better corrosion inhibition effect. This work provides a new strategy for improving bactericides and inhibiting MIC.

1. Introduction

Microbiologically influenced corrosion (MIC) is a special type of corrosion in which microorganisms directly or indirectly participate and lead to metal destruction and economic losses [1,2]. The cost associated with pitting corrosion incurred over $300,000 per unit per day for replacement cost [3]. Even stainless steel cannot be protected from pitting caused by MIC. Associated with most

* Corresponding author. Shandong Key Laboratory of Environmental Processes and Health, School of Environmental Science and Engineering, Shandong University, Qingdao, Shandong, 266237, China.
E-mail addresses: 202132988@mail.sdu.edu.cn (J. Zhou), lhy1007aaa@163.com (H. Li), 991352366@qq.com (S. Gong), wsg@sdu.edu.cn (S. Wang), xzyuan@sdu.edu.cn (X. Yuan), songchao@sdu.edu.cn (C. Song).

https://doi.org/10.1016/j.heliyon.2023.e21755
Received 13 August 2023; Received in revised form 27 September 2023; Accepted 27 October 2023
Available online 28 October 2023

MIC problems, sulfate reducing bacteria (SRB) is widely concerned in recent years [4–6], and it is generally considered to be the main bacterial group that causes metal corrosion in cooling water systems [7]. Moreover, SRB has been proven to cause and exacerbate pitting corrosion, and thus enhance the damage caused by stress corrosion cracking (SCC) on the pipeline [8]. Sulfate reduction in SRB cytoplasm requires biocatalysis and electrons, which are derived from extracellular iron oxidation and transferred to SRB cytoplasm through cell membrane. This electron transfer process is classified as extracellular electron transfer (EET), which is the main mechanism for MIC caused by SRB [9]. Furthermore, planktonic microorganisms in the liquid phase are usually not directly related to MIC, and the implementation of EET-MIC depends on biofilms, which are considered as the primary reason for MIC in most cases [10–12]. Therefore, the key to mitigating MIC is to reduce biofilms.

In many industrial systems, complete eradication of biofilms is impractical due to high doses of bactericides and long-term treatment. In addition, such treatment is also futile, as flow will bring back planktonic cells, leading to the biofilm formation again [12]. Moreover, biofilm exhibits natural defenses against external stress, such as slowing down the diffusion barrier of bactericide penetration [13]. Therefore, compared to planktonic cells, killing cells in a biofilm typically requires ten times or more bactericide doses [14]. Moreover, the addition of same bactericide repetitively can lead to microbial resistance, which also results in high demand for bactericide dosage [15]. Therefore, it is necessary to develop more effective methods to inhibit biofilm and enhance bactericide.

Recently, new bactericides have been developed to mitigate MIC caused by SRB. These bactericides exhibited excellent performances on MIC inhibition but with high dosages at hundreds ppm and intricate synthetic process, leading to high cost [16,17]. In contrast, it might be a low-cost and efficient strategy to enhance common bactericides via regulating biofilm. D-amino acids, a secretion widely found in many bacteria, exhibit significant impacts on biofilm formation. They can inhibit the formation of biofilms and promote the separation of biofilms [18,19]. Due to the wide distribution and biodegradability, D-amino acids are considered as a green and safe enhancer for bactericide [20–22]. For example, D-amino acids significantly enhanced the efficacy of bactericides via achieving at least an extra 2-log reduction of sessile cell counts [23]. Therefore, D-amino acids are also expected to be an excellent enhancer for bactericides to inhibit MIC. However, the mechanism of D-amino acid cooperating with bactericides for MIC inhibition is still unknown. Exploring the mechanism of D-amino acids as enhancers to mitigate MIC is significant for their application in the reduction of bactericides dosage.

In this study, D-tyrosine (D-Tyr) and disoctyl dimethyl ammonium chloride (DDAC) were selected as the typical D-amino acid and quaternary ammonium salt bactericide, respectively, to evaluate their roles in metal corrosion caused by SRB. The corrosion of Q235 steel was investigated via weight loss, electrochemical analysis, AFM and XRD. The formation of biofilm was determined to explore the synergy between D-Tyr and DDAC.

2. Materials and methods

2.1. Chemicals and material preparation

D-Tyr ($C_9H_{11}NO_3$, 98 %) and DDAC ($C_{18}H_{40}ClN$, 80 %) were both purchased from Shanghai Macklin Biochemical Co., Ltd. L-cysteine (>99 %) was purchased from Aladdin Holdings Group Co., Ltd, China. Unless otherwise specified, other reagents used in this study were analytical grade. The coupons used in this study were Q235 carbon steel, which is composed of C $\leq$ 0.20 %, Mn $\leq$ 1.4 %, Si $\leq$ 0.35 %, S $\leq$ 0.045, P $\leq$ 0.045 and balanced Fe. Coupons (10 $\times$ 10 $\times$ 3 mm) were first soaked in acetone and anhydrous ethanol for 3 min to remove surface grease and moisture. Then, these coupons were sequentially ground with 240, 400, and 600 grit sandpaper and exposed to ultraviolet light for 30 min for sterilization. Processed coupons were used for subsequent experiments.

2.2. Bacterial culture

In this study, *D. vulgaris* (ATCC 7757), a strain of SRB, was cultured with ATCC 1249 medium, which contained $MgSO_4$ 2.0 g/L, Sodium Citrate 5.0 g/L, $CaSO_4$ 0.79 g/L, NH_4Cl 1.0 g/L, K_2HPO_4 0.5 g/L, Sodium Lactate 3.5 g/L, and Yeast Extract 1.0 g/L (pH = 7.5 $\pm$ 0.2). The culture medium was first sterilized at 121 °C for 20 min, aerated with N_2 for 30 min, and then L-cysteine (100 mg/L) was added into the medium as a deoxidizer. According to pre-experiments (Fig. S1) and previous study, the concentrations of D-tyrosine and DDAC were set at 1 ppm and 5 ppm, respectively [24]. SRB was cultured in serum bottles containing 1 ppm D-tyrosine, 5 ppm DDAC, and 1 ppm D-tyrosine +5 ppm DDAC, labeled as D-Tyr, DDAC, and D-Tyr + DDAC, respectively. Control group was also designed without the addition of D-Tyr and DDAC. All groups were cultured at 30 °C, and optical density (OD) was recorded with a UV–vis Spectrophotometer (721, YOKE, Shanghai) at 600 nm. The concentration of SO_4^{2-} were measured with an ion chromatograph (ICS-6000, Thermo, USA) [25].

2.3. Analysis of weight loss and corrosion products

The coupons after 7-day incubation were collected, and corrosion products on the surface were scraped off gently and ground into powder for XRD (Ultima IV, Rigaku, Japan) analysis. Then, the coupons were soaked in the rust removal solution for 5 min to remove the residual corrosion products, and then weighed to calculate the weight loss. The corrosion degree is expressed with the annual corrosion depth (*Da* value) using the following equation:

$$Da=87600(W_0-W_1)/t\rho A \quad \text{eq(1)}$$

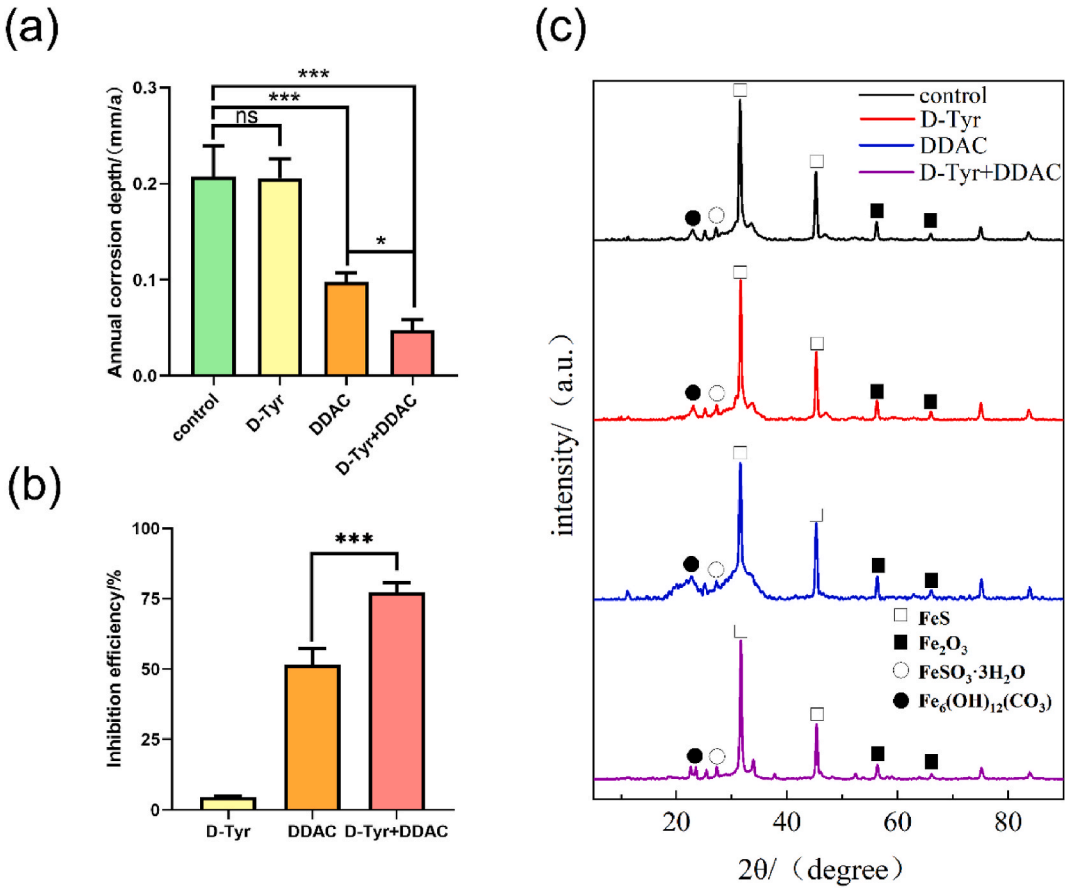

Fig. 1. Corrosion of the coupons after 7-day incubation: (a) Annual corrosion depth, (b) corrosion inhibition efficiency, and (c) XRD spectra of corrosion products.

where *Da* (mm/y) is annual corrosion depth; *t* (h) is soaking time; ρ (g/cm^3) is the density of Q235 carbon steel coupon; *A* (cm^2) is exposed surface area; W_0 (g) is the weight of the coupon before immersion; W_1 (g) is the weight of the coupon after immersion.

2.4. Corrosion pit analysis

The coupons in all groups were taken after 7-day incubation, and the biofilm on the surface was removed with ultrasound in deionized water for 5 min. Then, the coupons were soaked in rust removal solution (containing 500 mL hydrochloric acid, 500 mL deionized water and 3.5g hexamethylenetetramine) for 5 min to remove corrosion products from the surface. After lightly cleaned with 1 × PBS, the coupons were observed with AFM (Nano Wizard 4, Bruker, Germany) using a reported method [26]. At least 16 pits were analyzed in each group to calculate the depth and width of pits.

2.5. Electrochemical measurements

Electrochemical tests were conducted using a three-electrode sealed electrolytic cell and an electrochemical workstation (CHI660E, Gamry Instruments, USA). The reference electrode is a saturated calomel electrode, and the counter electrode is a platinum electrode. Q235 carbon steel coupons were welded with copper wire and sealed in epoxy resin, leaving 10 mm × 10 mm bare uncovered surface.

When the open circuit potential (OCP) is stable, electrochemical impedance spectroscopy (EIS) and Tafel curve measurements are performed. EIS data was obtained in the frequency range of 10^5 to 10^{-2} Hz [27]. The amplitude of the sinusoidal AC wave used is 5 mV. Different equivalent circuits in Zview software are used to fit the obtained EIS data. The polarization curve is measured in the potential range of −0.4 V to +0.4 V (compared to E_{OCP}), with a scan rate of 0.167 mV/s. Corrosion current densities (i_{corr}), polarization resistance (R_p) and anodic and cathodic Tafel slopes (β_a and β_c) were calculated from Tafel analyses of the polarization curves.

2.6. EPS analysis

EPS was extracted with the methods described by Tang et al. with some modification [6]. In brief, the culture medium cultured for 4

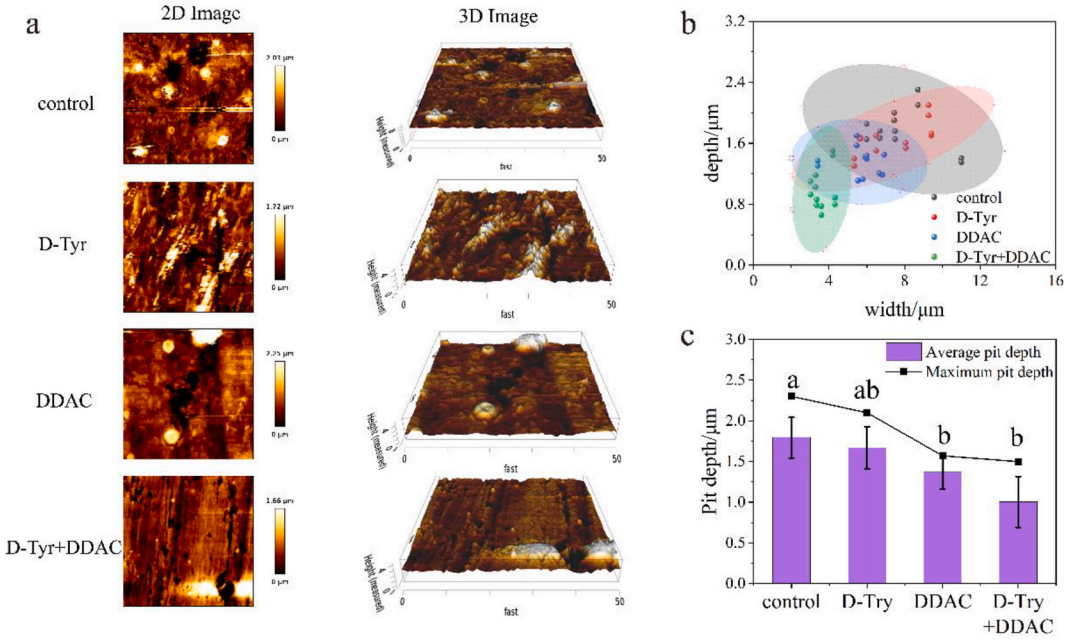

Fig. 2. Corrosion pit analysis with AFM: (a) 2D and 3D images of coupon surface, (b) distribution of corrosion pits, and (c) pit depth.

days was centrifuged at 8000 rpm for 3 min, and then the supernatant was removed. The sediment was cleaned twice with the 1 × PBS and heated in water bath at 70 °C for 60 min. After centrifuged at 11,000 rpm for 15 min, the supernatant was collected and filtered through 0.22 μm filters to obtain the sterile EPS solution for subsequent protein and polysaccharide determination. The protein (PN) and polysaccharide (PS) in EPS were measured with the modified Lowry method and anthrone method, respectively [28,29].

CLSM was applied to determine the distribution of EPS in the biofilm on coupons surface. Briefly, the coupons after 7-day incubation were collected and washed with 1 × PBS buffer to remove culture media, and planktonic cells before staining. The cleaned coupons were incubated in 100 μg/mL Alexa Flour 488 ConA (Invitrogen, Eugene, OR, USA) in dark for 30 min to stain the polysaccharide. The stained coupons were gently rinsed twice with 1 × PBS and then incubated with 1001 × Diluted SYPRO Orange (Invitrogen, Eugene, OR, USA) in dark for 30 min to stain protein. The stained coupons were gently rinsed twice with 1 × PBS. The coupons were mounted on a glass slide and visualized with a Confocal microscope (LSM 900 with Airyscan, ZEISS, Germany).

2.7. Biofilm analysis

The microstructure of the biofilm on the coupon surface was observed using a field emission electron microscope (SEM, Quanta 250 FEG, FEI, USA). Coupons in all groups were taken after 7-day incubation and immersed in 2.5 % glutaraldehyde (formulated with 1 × PBS) at 4 °C for 3 h. Then, the coupons were washed with 1 × PBS for 45 min. After that, the coupons were dehydrated with ethanol aqueous solution at a concentration gradient of 30 %, 50 %, 70 %, 80 %, and 90 % (v/v), with each step lasting for 15 min, and then dehydrated twice in 100 % ethanol for 15 min. After dried in a critical point dryer (EM CPD300, Leica, Germany), the surface of coupons was sputtered with gold to ensure conductivity for SEM analysis.

The growth activity of biofilm on the coupon surface was analyzed with a laser confocal microscope (LSM 900, ZEISS, Germany). Live and dead bacteria were stained with SYTO 9/PI Live/Dead Bacterial Double Stain Kit (Invitrogen, Eugene, OR, USA), and the excitation wavelengths were set at 488 and 561 nm, respectively [30]. In order to analyze the thickness and morphology of the biofilm, the coupons were immersed in 2 % glutaraldehyde at 48 °C for 2 h, dehydrated in ethanol solution (25 %, 50 %, 75 %, and 100 %) for 5 min in turn, and then dried overnight in a dryer. Then, the coupons were observed with LSM 900 in 3D mode [31].

3. Results and discussion

3.1. Analysis of weight loss and corrosion products

Weight loss of coupons can reflect the degree of corrosion directly, and the annual corrosion depth and corrosion inhibition efficiency were calculated according to corrosion weight loss. As shown in Fig. 1a, D-Tyr exhibited negligible impact on the annual corrosion depth and corrosion inhibition efficiency, while DDAC reduced the annual corrosion depth by 53.47 %. In D-Tyr + DDAC group, annual corrosion depth decreased to 0.047 ± 0.011mm/a with high corrosion inhibition efficiency, up to 77.23 % (Fig. 1b). These results indicate that D-Tyr could well enhance the role of DDAC in corrosion inhibition. Recently, some new bactericides were developed to inhibit the MIC caused by SRB with high inhibition efficiencies above 85 % [32,33]. For example, corrosion was

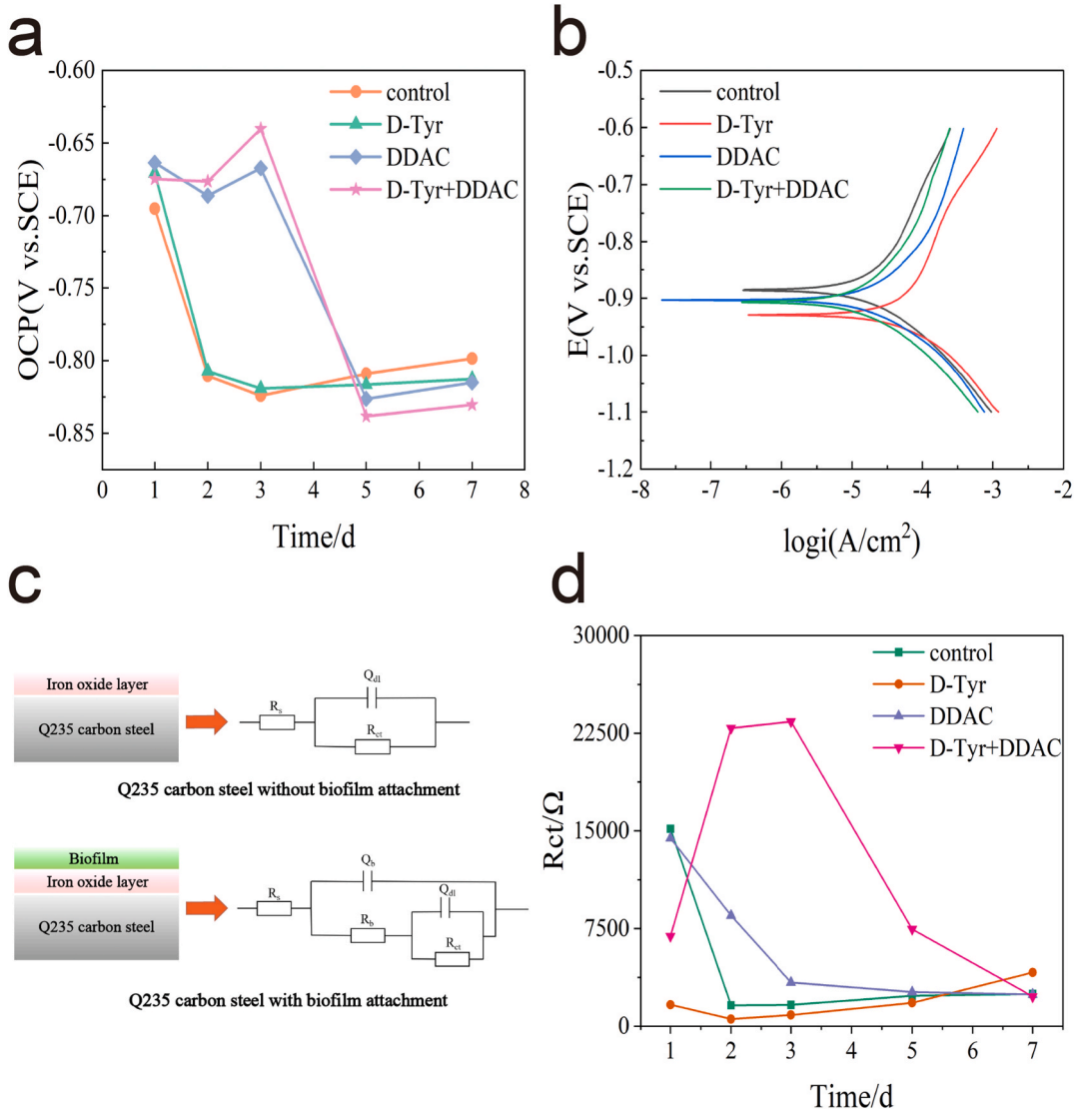

Fig. 3. Electrochemical tests of Q235 samples immersed in different culture media; (a) open circuit potential, (b) polarization curve after 7-day incubation, (c) equivalent circuits used for fitting EIS data and (d) R_{ct}.

obviously inhibited by 96.3 % in the presence of Schiff base cationic surfactants at 2000 ppm [33]. Compared to these studies, lower corrosion inhibition was obtained in this study, but the dosages of D-Try and DDAC were only 1 ppm and 5 ppm, respectively, which are far less than the new bactericides. Besides, DDAC is a common bactericide widely used in industrial water treatment, implying the low cost of corrosion inhibitors in this study. Furthermore, corrosion products were analyzed with XRD (Fig. 1c). Strong signals at 31.5° and 45.22°were detected in all groups, suggesting that FeS was the primary corrosion products and the coupon surface was strongly attacked by biological sulfides [34]. Weak peaks were also observed at 22.88° and 27.16°, which were ascribed to $Fe_6(OH)_{12}(CO_3)$ and $FeSO_3{\cdot}H_2O$, respectively [35]. The signals of Fe_2O_3 were also detected at 56.22° and 66.02° with low intensity, resulting from the low content of Fe_2O_3 due to anaerobic environment in this study [36]. It is noting that the components of corrosion products were similar in all groups, implying that both D-Tyr and DDAC did not change the corrosion mechanism of SRB. Their approach to inhibiting corrosion may be attribute to reduce the number of bacteria and bacterial activity.

3.2. Surface analysis

Microscopic morphology of coupons was observed with AFM and SEM after removing corrosion products (Fig. 2 and Fig. S2). Large circular corrosion pits were observed in control group and D-Tyr group, and their number decreased in the presence of DDAC. Whereas, only small corrosion pits were detected in D-Tyr + DDAC group. Moreover, the depth and width of at least 16 pits in each group were listed in Fig. 2b. The width and depth of pits decreased in DDAC group. The addition of D-tyrosine significantly enhanced this trend,

Table 1
Electrochemical parameters fitted from the polarization curves of coupons after 7-day incubation.

Group	β_a	β_c	i_{corr} (μA/cm^2)	R_p/Ω
Control	112.36	−241.55	22.62	1474
D-Tyr	114.13	−199.08	26.39	1195
DDAC	110.23	−168.12	21.60	1340
D-Tyr + DDAC	110.58	−192.98	14.40	2123

resulting in small and shallow pits on coupon surface. The average pit depth in control group is 1.79 ± 0.25 μm with the maximum depth at 2.30 μm while it is 1.37 ± 0.20 μm and 1.00 ± 0.31 μm with maximum pit depth at 1.57 μm and 1.5 μm in DDAC group and D-Tyr + DDAC group, respectively. These results indicate that D-tyrosine obviously enhanced the roles of DDAC in corrosion inhibition, leading to a significant reduction in the number, average depth and width of corrosion pits. It is consisted with weight loss analysis.

3.3. Electrochemical analysis

Various electrochemical tests were conducted to evaluate the impact of D-Tyr and DDAC on corrosion process. OCP was first performed to reflect the thermodynamic corrosion tendency of coupon surface [37]. As shown in Fig. 3a, a rapid decrease in OCP values was observed on the second day in groups without DDAC, indicating that the coupon surface changed to be conducive to corrosion reaction in thermodynamic [38]. It is mainly attributed to the gradual attachment of cells. The OCP values kept stable in the first three days and the decreased rapidly on the 5th day in DDAC group and D-Tyr + DDAC group, implying the delayed corrosion of coupons due to the roles of DDAC and D-Tyr in biofilm inhibition. Furthermore, the corrosion potential in each group was similar (Fig. 3b), which is consistent with the trend of OCP at 7th day. Electrochemical parameters, including anodic Tafel slope (β_a), cathodic Tafel slope (β_c), corrosion current density (i_{corr}) and polarization resistance (R_p), were also calculated by fitting Tafel curve (Table 1) [39]. Similar β_a were obtained in all groups while β_c decreased obviously in the presence of DDAC or D-Tyr, suggesting the inhibition of cathode reaction. Cathode depolarization is considered as one of the most important mechanism of SRB-induced corrosion [40]. Therefore, DDAC and D-Tyr mainly acted on SRB and thus inhibited cathode reaction. Generally, corrosion current is positively associated with corrosion reaction rate [41]. In DDAC group, i_{corr} was 21.60 μA/cm^2, close to that of control group (22.62 μA/cm^2), indicating that the role of DDAC in corrosion inhibition was negligible on the 7th day. However, i_{corr} was only 14.4 μA/cm^2 in D-Tyr + DDAC group, suggesting less corrosion occurred on the 7th day. Besides, a corresponding increase in R_p was also detected as the decrease of current density. These results confirm that D-Tyr could enhance the inhibition of DDAC on SRB-induced corrosion.

Furthermore, electrochemical impedance spectroscopy and charge transfer resistance (R_{ct}) were obtained to further explore the corrosion. As shown in Fig. S3, the maximum low-frequency capacitive arc radiuses were detected in D-Tyr + DDAC group at the most time of the incubation. suggesting that the coupons are not easy to lose electrons and exhibit strong corrosion resistance [42]. Besides, The EIS results were fitted using the equivalent circuit diagram shown in Fig. 3c. R_s represents the solution resistance, while Q_f and R_f represent the capacitance and resistance of membranes composed of corrosion products and biofilms, respectively. Q_{dl} and R_{ct} represent double layer capacitors and charge transfer resistors, respectively. R_{ct} is closely related to the electrochemical property of coupon surface, which is manly attributed to the attachment of bacteria on the surface in this study. As shown in Fig. 3d, the D-Tyr + DDAC group detected significantly higher R_{ct} values than other groups for most of the time. The change trend of R_{ct} in the control group is first increasing and then decreasing, corresponding to the formation of biofilm and the accumulation of corrosion products, respectively [43]. The fitted R_{ct} values confirm the previous judgment that the mixed treatment of D-tyrosine and DDAC achieved outstanding anti-corrosion effect.

3.4. The effect of D-Tyr on SBR growth

In this study, D-tyrosine exhibited negligible effect on corrosion caused by SRB when added alone, but it enhanced obviously the role of DDAC in corrosion inhibition. There might be three reasons for these results: a) D-Tyr improved the toxicity of DDAC and thus reduced the biomass of SRB; b) the capacity of SRB obtaining electron from Fe was inhibited in the presence of DDAC and D-Tyr; c) D-tyrosine inhibited the EPS secretion and biofilm formation, and thus decreased the resistance of cells to DDAC. To verified these speculations, the activity of planktonic SRB was first evaluated to explore the toxicity of DDAC in the presence of D-Tyr. As shown in Fig. 4a, little change of biomass was detected in the presence of D-Tyr whether DDAC was added or not, indicating that D-tyrosine did not enhance the bactericidal effect of DDAC on SRB. Besides, a delay of bacterial growth was observed with the addition of DDAC at the first 3 days, and then SRB grew rapidly with slightly higher biomass than control group. It could well explain the results of OCP values that the delayed corrosion of coupons in the first 3 days (Fig. 3a). Moreover, SO_4^{2-}, the primary electron acceptor for SRB, was selected to evaluate the capacity of SRB obtaining electron from Fe [6]. The utilization of SO_4^{2-} was delayed by 3 days in the presence of DDAC (Fig. 4b), which is consisted with the growth of SRB. Besides, little change was observed with the addition of D-Tyr, suggesting that D-Tyr could not inhibit the capacity of SRB obtaining electron from Fe.

3.5. EPS and biofilm analysis

EPS, mainly composed of polysaccharides and proteins, are considered as excellent protections for bacterial cells from toxic

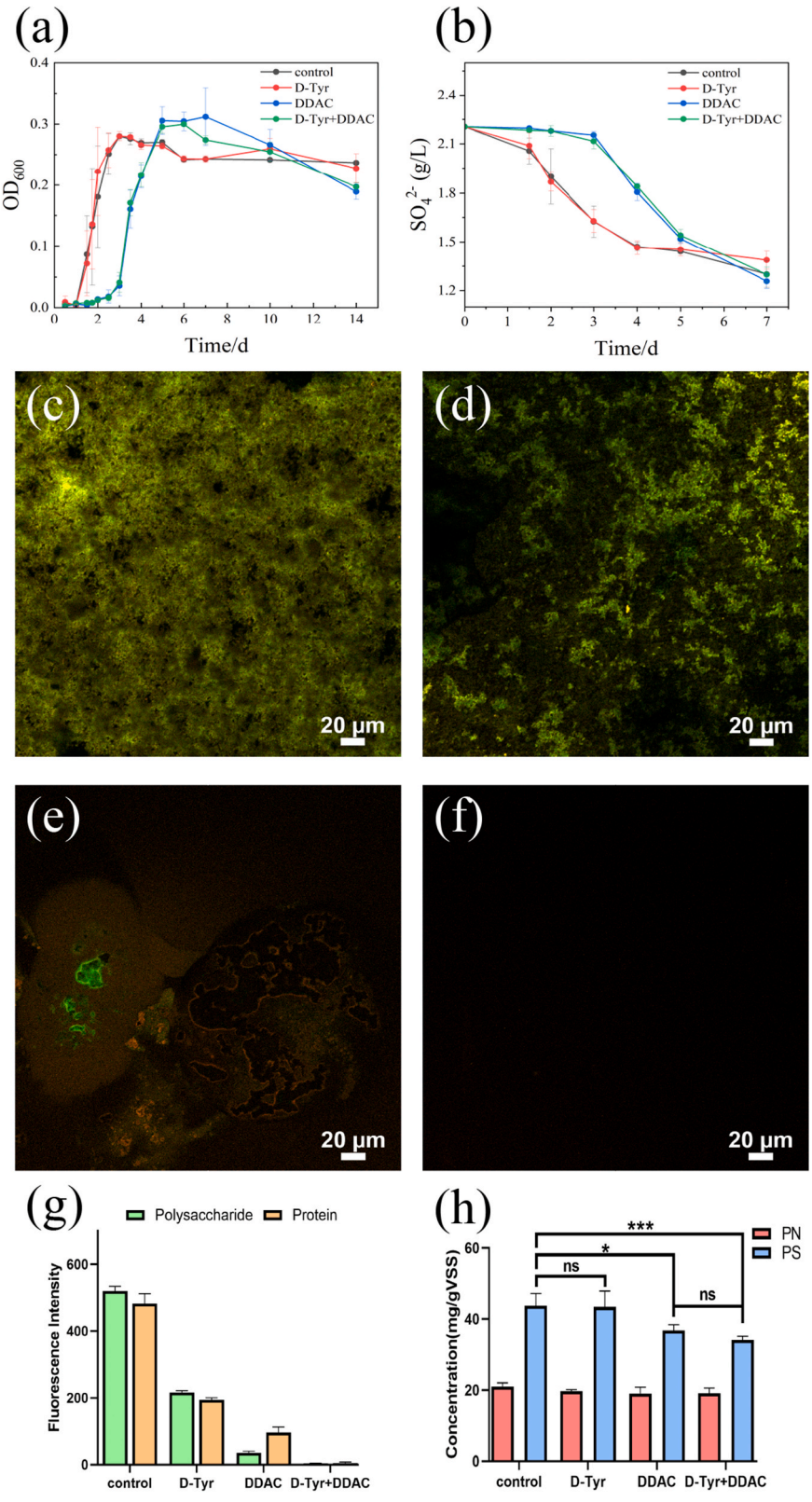

(caption on next page)

Fig. 4. The growth curve of SRB (a), the concentration of sulfate in medium during incubation (b), CLSM images of polysaccharides and proteins on coupon surface (c–f), fluorescence intensity (g) and EPS secretion of planktonic bacteria (h)after 7-day incubation: control group (c), D-Tyr group (d), DDAC group (e) and D-Tyr + DDAC group (f). In the CLSM images, polysaccharide and protein was stained in green and orange respectively. (For interpretation of the references to colour in this figure legend, the reader is referred to the Web version of this article.)

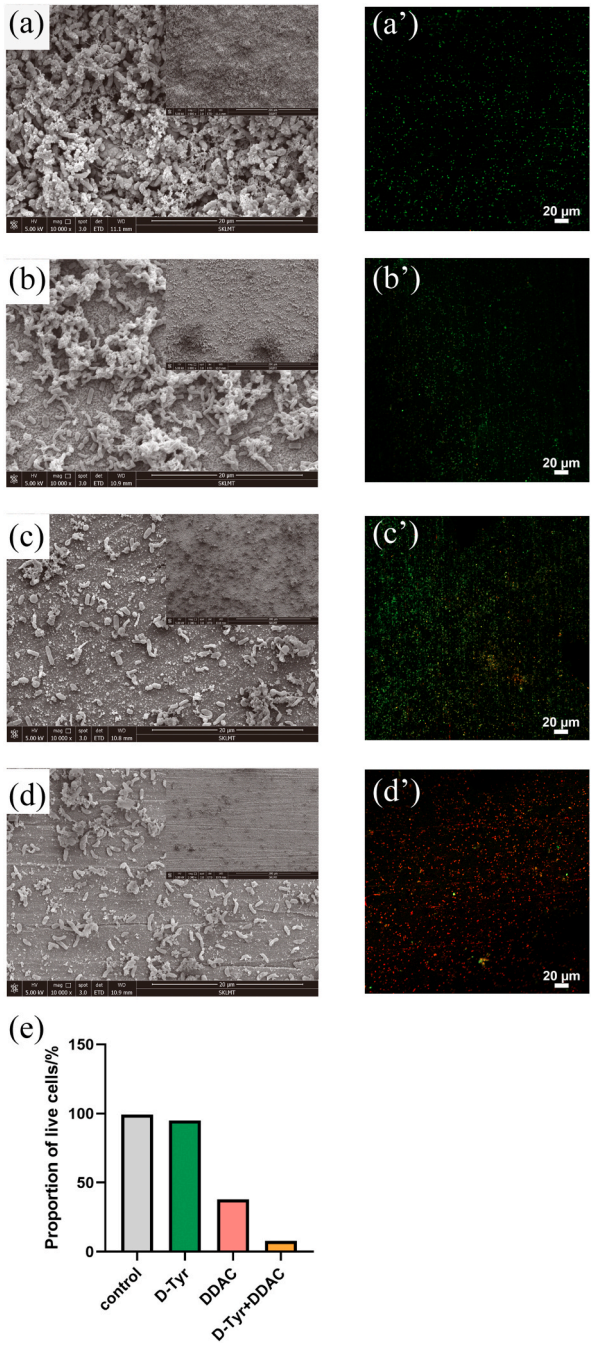

Fig. 5. SEM and fluorescence staining images of coupon surface after 7-day incubation in control group (a, a'), D-Tyr group (b, b'), DDAC group (c, c') and D-Tyr + DDAC group (d, d') and the proportion of live bacteria calculated based on the total number of cells in at least five confocal images (e). SEM images and illustrations show microscopic images at 10000x and 1000x magnification, respectively. In fluorescence staining images, live cells and dead cells were stained in green and red, respectively.

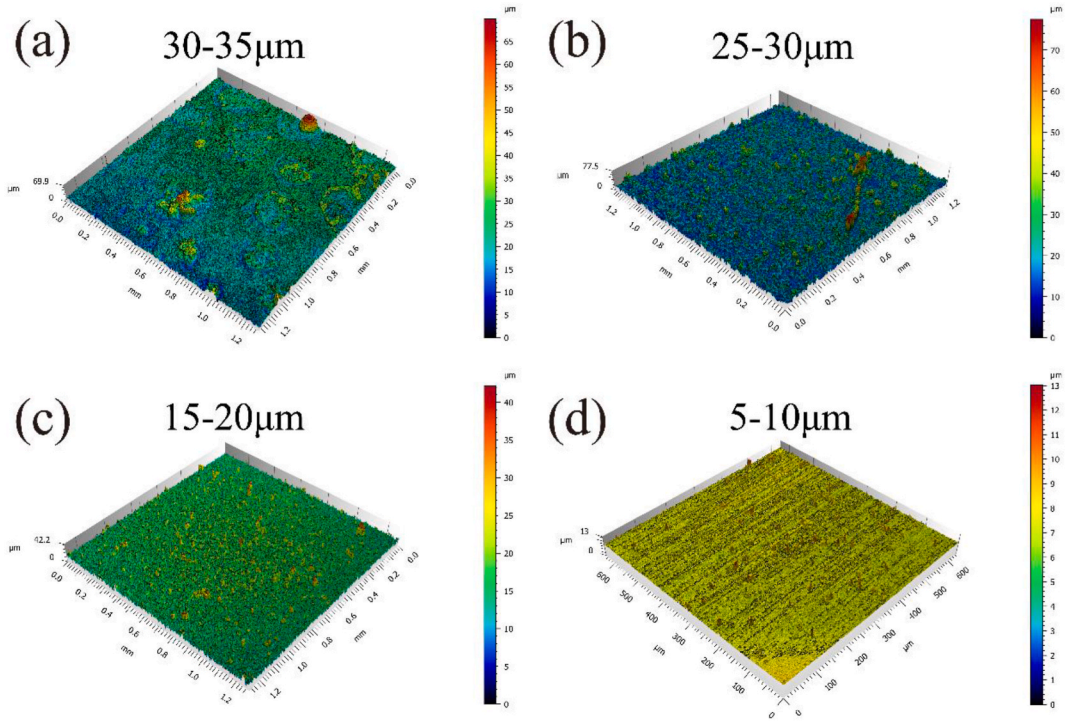

Fig. 6. CLSM layer scanning images of biofilm on the coupon surface after 7-day incubation in control group (a), D-Tyr group (b), DDAC group (c) and D-Tyr + DDAC group (d).

substance [14]. Therefore, the secretion of EPS was investigated after 4-day incubation in this study. Little difference was detected in protein content between the four groups (Fig. 4h), indicating that both DDAC and D-Tyr exhibited little effect on the secretion of extracellular protein. DDAC resulted in a slight decrease in PS production, but there is no significant difference in PS between DDAC group and D-Tyr + DDAC group. These results indicate that D-Tyr played a negligible role in EPS secretion. Furthermore, EPS are also indispensable components of biofilm and play an important role in bacterial attachment. In this study, CLSM was applied to investigate the distribution of EPS on the coupon surface (Fig. 4c–f and Fig. S4). In control group, coupons were almost covered by PN and PS, suggesting the coverage of biofilm on the coupons. The content of PN and PS decreased obviously in D-Tyr group, which might be due to the role of D-Tyr in bacterial attachment [44]. Only a small amount of PN and PS was observed in DDAC group, and their distribution was chaotic and dispersive due to the bactericidal activity of DDAC. Besides, almost no PN and PS were detected on coupon surface in D-Tyr + DDAC group, indicating that little live cells attached on the surface. In conclusion, the combine of DDAC and D-Tyr exhibited little impact on the secretion of EPS but decreased the distribution of EPS on the coupon surface, which would reduce the attachment of cells and the formation of biofilm on the surface.

Furthermore, the biofilm formation of SRB on coupon surface was observed with SEM. As shown in Fig. 5a–d, there were rod-shaped cells on the coupon, and white substances were also observed on the bacterial surface, which might be EPS secreted by SRB. The coupons were fully covered with biofilm in control group (Fig. 5a), and D-tyrosine resulted in partial detachment of biofilm and reduced the coverage area (Fig. 5b). In the presence of DDAC, the amount of bacteria significantly decreased, and there was almost no EPS observed on coupon surface, especially in D-Tyr + DDAC group (Fig. 5c and d), which is consistent with EPS analysis. Moreover, CLSM was applied to evaluate the distribution of live and dead cells on the coupons (Fig. 5a'-d'), and the proportion of live cells was calculated with ImageJ software (Fig. 5e) [45]. Almost all cells were alive in control group and D-Tyr group (>90 %), confirming the negligible impact of D-Tyr on SRB growth. In DDAC group, dead cells covered most areas of the coupons while dense aggregation of live cells was observed in a few areas with the total proportion of live cells at 37.91 % (Fig. 5c'). It indicates that there was still small biofilm formed on the coupons and protecting cells from DDAC. However, more than 92 % of cells were killed on the coupons without any biofilm in the presence of DDAC and D-Tyr (Fig. 5d'), suggesting that D-Tyr inhibited the formation of biofilm and thus decreased the resistance of cells to DDAC [46]. These results could well explain the low i_{corr} detected in D-Tyr + DDAC group (Table 1), where almost all cells on the coupons died without biofilm, resulting in a significant decrease in corrosion current. Moreover, the thickness of biofilm was determined using CLSM layer scanning with the confocal microscope Z-stack mode (Fig. 6). Thick biofilm was detected in control group and D-Tyr group with average thickness at 30–35 μm and 25–30 μm, respectively. There was a small amount of blocky protrusions on coupon surfaces, resulting from corrosion product. Coupon surfaces became relatively flat (average thickness at 15–20 μm) with a few protrusions in DDAC group (Fig. 6c), which is consistent with the corrosion pit analysis. In D-Tyr + DDAC group, there was little biofilm on the coupons with average thickness at 5–10 μm without any protrusions, which was attributed to the sedimentation of dead cells (Fig. 6d). These results confirm the biofilm inhibition by the combine of D-Tyr and DDAC, which were also

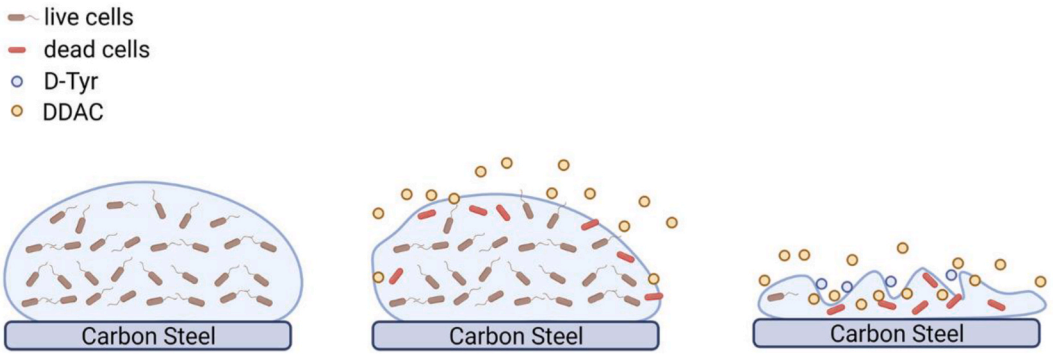

Fig. 7. The mechanism of D-Tyr enhancing the role of DDAC in corrosion inhibition.

consistent with EPS analysis (Fig. 4) and SEM (Fig. 5). In conclusion, D-Tyr could decrease the attachment of EPS and live cells on the coupon surface, which would be the main reason for enhancing DDAC on corrosion inhibition.

3.6. The mechanism of D-Tyr enhancing DDAC on corrosion inhibition

Biofilm is an ancient and widespread form of life in natural and artificial environment, where bacteria attach to the metal surface through quorum sensing and cause MIC [47–49]. Bactericides are common agents for MIC inhibition but exhibit weak bactericidal performance to cells in biofilm due to their strong resistance [14]. Our previous studies found that D-amino acid could reduce bacterial adhesion and decompose biofilms, leading to bacteria exposure to external adverse environments [27,44]. In this study, D-tyrosine obviously enhanced the inhibition of DDAC on SRB-induced MIC, and their synergistic mechanism were well explored (Fig. 7): D-tyrosine could not inhibit the bacterial growth, EPS secretion and the capacity of SRB obtaining electron from Fe. However, D-tyrosine could decrease the attachment of EPS and live cells on the coupon surface, and thus inhibit the formation of biofilm, leading to more cells directly exposed to DDAC. It decreased the amount of live cells and thus reduced the utilization of Fe by SRB and corrosion current on the coupon surface. Moreover, dead cells settling to the coupon surface may form a protective lay to retard the contact between live SRB and Fe, leading to slow cathode reaction and less corrosion.

4. Conclusions

The combination of D-Tyr and DDAC significantly inhibits the corrosion process and reduces the size of the corrosion pit and corrosion current on the coupon surface. D-tyrosine could decrease the attachment of EPS and live cells on the coupon surface, inhibit the formation of biofilm, and make more cells directly exposed to DDAC. The reduction of live cells on the coupon surface also decreased the utilization of Fe by SRB. Moreover, dead cells settling to the coupon surface may form a protective lay to retard the contact between live SRB and Fe, which also inhibited the corrosion. This work provides a low-cost and efficient strategy to mitigate MIC.

Data availability statement

Data will be made available on request.

CRediT authorship contribution statement

Jingyi Zhou: Formal analysis, Investigation, Methodology, Validation, Writing – original draft, Writing – review & editing. **Hongyi Li:** Formal analysis, Methodology, Validation, Writing – original draft. **Shichu Gong:** Formal analysis, Methodology, Validation, Writing – original draft. **Shuguang Wang:** Formal analysis, Writing – review & editing, Resources. **Xianzheng Yuan:** Resources, Writing – review & editing. **Chao Song:** Conceptualization, Formal analysis, Methodology, Resources, Supervision, Writing – original draft, Writing – review & editing.

Declaration of competing interest

The authors declare that they have no known competing financial interests or personal relationships that could have appeared to influence the work reported in this paper.

Acknowledgments

This work was supported by the National Natural Science Foundation of China (U20A20146 and 22378232), the Young Scholars

Program of Shandong University and Taishan Scholars Project of Shandong Province (NO. tstp20230604). We thank Haiyan Yu, Xiaomin Zhao and Yuyu Guo, Sen Wang from Core Facilities for Life and Environmental Sciences of SKLMT (State Key Laboratory of Microbial Technology, Shandong University) for assistance in microscopy imaging of CLSM and SEM.

Appendix A. Supplementary data

Supplementary data to this article can be found online at https://doi.org/10.1016/j.heliyon.2023.e21755.

References

[1] E. Zhou, H. Li, C. Yang, J. Wang, D. Xu, D. Zhang, T. Gu, Accelerated corrosion of 2304 duplex stainless steel by marine Pseudomonas aeruginosa biofilm, Int. Biodeterior. Biodegrad. 127 (2018) 1–9.
[2] C.A. Loto, Microbiological corrosion: mechanism, control and impact—a review, Int. J. Adv. Des. Manuf. Technol. 92 (2017) 4241–4252.
[3] I.B. Beech, C.C. Gaylarde, Recent advances in the study of biocorrosion - an overview, Rev. Microbiol. 30 (1999) 177–190.
[4] T. Gu, R. Jia, T. Unsal, D. Xu, Toward a better understanding of microbiologically influenced corrosion caused by sulfate reducing bacteria, J. Mater. Sci. Technol. 35 (2019) 631–636.
[5] D. Wang, J. Liu, R. Jia, W. Dou, S. Kumseranee, S. Punpruk, X. Li, T. Gu, Distinguishing two different microbiologically influenced corrosion (MIC) mechanisms using an electron mediator and hydrogen evolution detection, Corrosion Sci. 177 (2020), 108993.
[6] M. Tang, S. Zhou, J. Huang, L. Sun, H. Lu, Stress responses of sulfate-reducing bacteria sludge upon exposure to polyethylene microplastics, Water Res. 220 (2022), 118646.
[7] R. Liang, J. Li, M. Liu, Z.Y. Huang, Influence of inhibitors on the adhesion of SRB to the stainless steel in circulating cooling water, Colloids Surf. B Biointerfaces 172 (2018) 1–9.
[8] S.S. Abedi, A. Abdolmaleki, N. Adibi, Failure analysis of SCC and SRB induced cracking of a transmission oil products pipeline, Eng. Fail. Anal. 14 (2007) 250–261.
[9] R. Jia, D. Yang, H.B. Abd Rahman, T. Gu, An enhanced oil recovery polymer promoted microbial growth and accelerated microbiologically influenced corrosion against carbon steel, Corrosion Sci. 139 (2018) 301–308.
[10] D. Xu, T. Gu, Carbon source starvation triggered more aggressive corrosion against carbon steel by the Desulfovibrio vulgaris biofilm, Int. Biodeterior. Biodegrad. 91 (2014) 74–81.
[11] R. Jia, T. Unsal, D. Xu, Y. Lekbach, T. Gu, Microbiologically influenced corrosion and current mitigation strategies: a state of the art review, Int. Biodeterior. Biodegrad. 137 (2019) 42–58.
[12] D. Xu, R. Jia, Y. Li, T. Gu, Advances in the treatment of problematic industrial biofilms, World J. Microbiol. Biotechnol. 33 (2017) 97.
[13] R. Jia, D. Yang, Y. Li, D. Xu, T. Gu, Mitigation of the Desulfovibrio vulgaris biofilm using alkyldimethylbenzylammonium chloride enhanced by d-amino acids, Int. Biodeterior. Biodegrad. 117 (2017) 97–104.
[14] T.-F.C. Mah, G.A. O'Toole, Mechanisms of biofilm resistance to antimicrobial agents, Trends Microbiol. 9 (2001) 34–39.
[15] E.A. Saverina, N.A. Frolov, O.A. Kamanina, V.A. Arlyapov, A.N. Vereshchagin, V.P. Ananikov, From antibacterial to antibiofilm targeting: an emerging paradigm shift in the development of quaternary ammonium compounds (QACs), ACS Infect. Dis. 9 (2023) 394–422.
[16] L. Katebian, E. Gomez, L. Skillman, D. Li, G. Ho, S.C. Jiang, Inhibiting quorum sensing pathways to mitigate seawater desalination RO membrane biofouling, Desalination 393 (2016) 135–143.
[17] T. Ergön-Can, B. Köse-Mutlu, İ. Koyuncu, C.-H. Lee, Biofouling control based on bacterial quorum quenching with a new application: rotary microbial carrier frame, J. Membr. Sci. 525 (2017) 116–124.
[18] H. Xu, Y. Liu, d-Amino acid mitigated membrane biofouling and promoted biofilm detachment, J. Membr. Sci. 376 (2011) 266–274.
[19] C. Yu, X. Li, N. Zhang, D. Wen, C. Liu, Q. Li, Inhibition of biofilm formation by d-tyrosine: effect of bacterial type and d-tyrosine concentration, Water Res. 92 (2016) 173–179.
[20] X. Liu, Z. Li, Y. Fan, Y. Lekbach, Y. Song, D. Xu, Z. Zhang, L. Ding, F. Wang, A mixture of D-amino acids enhances the biocidal efficacy of CMIT/MIT against corrosive Vibrio harveyi biofilm, Front. Microbiol. 11 (2020).
[21] J. Xu, R. Jia, D. Yang, C. Sun, T. Gu, Effects of d-Phenylalanine as a biocide enhancer of THPS against the microbiologically influenced corrosion of C1018 carbon steel, J. Mater. Sci. Technol. 35 (2019) 109–117.
[22] R. Jia, D. Yang, D. Xu, T. Gu, Carbon steel biocorrosion at 80 °C by a thermophilic sulfate reducing archaeon biofilm provides evidence for its utilization of elemental iron as electron donor through extracellular electron transfer, Corrosion Sci. 145 (2018) 47–54.
[23] R. Jia, D. Yang, H.H. Al-Mahamedh, T. Gu, Electrochemical testing of biocide enhancement by a mixture of d-amino acids for the prevention of a corrosive biofilm consortium on carbon steel, Ind. Eng. Chem. Res. 56 (2017) 7640–7649.
[24] T. Unsal, D. Wang, S. Kumseranee, S. Punpruk, T. Gu, d-Tyrosine enhancement of microbiocide mitigation of carbon steel corrosion by a sulfate reducing bacterium biofilm, World J. Microbiol. Biotechnol. 37 (2021) 103.
[25] K. Shi, W. Cheng, Q. Jiang, J. Xue, Y. Qiao, D. Cheng, Insight of the bio-cathode biofilm construction in microbial electrolysis cell dealing with sulfate-containing wastewater, Bioresour. Technol. 361 (2022), 127695.
[26] J. Narenkumar, P. Elumalai, S. Subashchandrabose, M. Megharaj, R. Balagurunathan, K. Murugan, A. Rajasekar, Role of 2-mercaptopyridine on control of microbial influenced corrosion of copper CW024A metal in cooling water system, Chemosphere 222 (2019) 611–618.
[27] H. Li, Z. Kang, K. Zhang, S. Gong, X. Zhao, Z. Yan, S. Wang, C. Song, Enhanced inhibition of HEDP on SRB-mediated corrosion with D-phenylalanine, Environ. Res. 227 (2023), 115754.
[28] H. Zhang, Y. Jia, S.K. Khanal, H. Lu, H. Fang, Q. Zhao, Understanding the role of extracellular polymeric substances on ciprofloxacin adsorption in aerobic sludge, anaerobic sludge, and sulfate-reducing bacteria sludge systems, Environ. Sci. Technol. 52 (2018) 6476–6486.
[29] B. Frølund, R. Palmgren, K. Keiding, P.H. Nielsen, Extraction of extracellular polymers from activated sludge using a cation exchange resin, Water Res. 30 (1996) 1749–1758.
[30] Z. Li, J. Zhou, X. Yuan, Y. Xu, D. Xu, D. Zhang, D. Feng, F. Wang, Marine biofilms with significant corrosion inhibition performance by secreting extracellular polymeric substances, ACS Appl. Mater. Interfaces 13 (2021) 47272–47282.
[31] G. Chilkoor, K. Jawaharraj, B. Vemuri, A. Kutana, M. Tripathi, D. Kota, T. Arif, T. Filleter, A.B. Dalton, B.I. Yakobson, M. Meyyappan, M.M. Rahman, P. M. Ajayan, V. Gadhamshetty, Hexagonal boron nitride for sulfur corrosion inhibition, ACS Nano 14 (2020) 14809–14819.
[32] S.M. Tawfik, A.S. Kobisy, E.A. Badr, A.H. Elged, Y.-I. Lee, Surface-active nonionic conjugated zirconium metal–organic frameworks and their applications; Broad spectrum anti-microbial, anti-SRB biofilm, anti-microbial corrosion, Environmental Technology & Innovation 29 (2023), 103001.
[33] A.S. Kobisy, H.N. Nassar, S.M. Tawfik, E.H. Elshatoury, I. Aiad, Mitigation of eco-unfriendly and costly microbial induced corrosion using novel synthesized Schiff base cationic surfactants, Journal of Chemical Technology & Biotechnology 96 (2021) 941–952.
[34] R. Jia, D. Wang, P. Jin, T. Unsal, D. Yang, J. Yang, D. Xu, T. Gu, Effects of ferrous ion concentration on microbiologically influenced corrosion of carbon steel by sulfate reducing bacterium Desulfovibrio vulgaris, Corrosion Sci. 153 (2019) 127–137.

[35] L. Xu, F. Guan, Y. Ma, R. Zhang, Y. Zhang, X. Zhai, X. Dong, Y. Wang, J. Duan, B. Hou, Inadequate dosing of THPS treatment increases microbially influenced corrosion of pipeline steel by inducing biofilm growth of Desulfovibrio hontreensis SY-21, Bioelectrochemistry 145 (2022), 108048.
[36] P. Silva, S.H. Oliveira, G.M. Vinhas, L.J. Carvalho, O.S. Baraúna, S.L. Urtiga Filho, M.A.G.A. Lima, Tetrakis hydroxymethyl phosphonium sulfate (THPS) with biopolymer as strategy for the control of microbiologically influenced corrosion in a dynamic system, Chemical Engineering and Processing - Process Intensification 160 (2021), 108272.
[37] T. Unsal, D. Wang, S. Kumseranee, S. Punpruk, M.E.-S. Mohamed, M.A. Saleh, T. Gu, Assessment of 2,2-dibromo-3-nitrilopropionamide biocide enhanced by D-tyrosine against zinc corrosion by a sulfate reducing bacterium, Ind. Eng. Chem. Res. 60 (2021) 4009–4018.
[38] M. Moradi, Y. Yang, D. Xu, Z. Song, F. Wang, Interspecies interactions of Vibrio azureus and Jeotgalibacillus alkaliphilus on corrosion of duplex stainless steel, Int. Biodeterior. Biodegrad. 160 (2021), 105212.
[39] R. Jia, D. Yang, J. Xu, D. Xu, T. Gu, Microbiologically influenced corrosion of C1018 carbon steel by nitrate reducing Pseudomonas aeruginosa biofilm under organic carbon starvation, Corrosion Sci. 127 (2017) 1–9.
[40] A.K. Tripathi, P. Thakur, P. Saxena, S. Rauniyar, V. Gopalakrishnan, R.N. Singh, V. Gadhamshetty, E.Z. Gnimpieba, B.K. Jasthi, R.K. Sani, Gene sets and mechanisms of sulfate-reducing bacteria biofilm formation and quorum sensing with impact on corrosion, Front. Microbiol. 12 (2021).
[41] G. Chilkoor, S.P. Karanam, S. Star, N. Shrestha, R.K. Sani, V.K.K. Upadhyayula, D. Ghoshal, N.A. Koratkar, M. Meyyappan, V. Gadhamshetty, Hexagonal boron nitride: the thinnest insulating barrier to microbial corrosion, ACS Nano 12 (2018) 2242–2252.
[42] B. Liu, M. Sun, F. Lu, C. Du, X. Li, Study of biofilm-influenced corrosion on X80 pipeline steel by a nitrate-reducing bacterium, Bacillus cereus, in artificial Beijing soil, Colloids Surf. B Biointerfaces 197 (2021), 111356.
[43] M. Moradi, G. Ghiara, R. Spotorno, D. Xu, P. Cristiani, Understanding biofilm impact on electrochemical impedance spectroscopy analyses in microbial corrosion and microbial corrosion inhibition phenomena, Electrochim. Acta 426 (2022), 140803.
[44] H. Li, Y. Wang, X. Zhao, Z. Yan, C. Song, S. Wang, Chirality of tyrosine controls biofilm formation via the regulation of bacterial adhesion, Biochem. Eng. J. 192 (2023), 108844.
[45] R. Jia, D. Yang, D. Xu, T. Gu, Mitigation of a nitrate reducing Pseudomonas aeruginosa biofilm and anaerobic biocorrosion using ciprofloxacin enhanced by D-tyrosine, Sci. Rep. 7 (2017) 6946.
[46] D. Xu, Y. Li, T. Gu, A synergistic d-tyrosine and tetrakis hydroxymethyl phosphonium sulfate biocide combination for the mitigation of an SRB biofilm, World J. Microbiol. Biotechnol. 28 (2012) 3067–3074.
[47] H.-C. Flemming, J. Wingender, The biofilm matrix, Nat. Rev. Microbiol. 8 (2010) 623–633.
[48] B. Xu, T.C.A. Ng, S. Huang, M. He, S. Varjani, H.Y. Ng, Quorum quenching affects biofilm development in an anaerobic membrane bioreactor (AnMBR): from macro to micro perspective, Bioresour. Technol. 344 (2022), 126183.
[49] K. Lee, H. Yu, X. Zhang, K.-H. Choo, Quorum sensing and quenching in membrane bioreactors: opportunities and challenges for biofouling control, Bioresour. Technol. 270 (2018) 656–668.